Inelastic neutron scattering from confined molecular oxygen

Duncan Kilburn,[1] Paul E. Sokol,[1] and Craig M. Brown[2]
[1]*Indiana University Cyclotron Facility, 2401 Milo B. Sampson Lane, Bloomington, Indiana 47404, USA*
[2]*NIST Center for Neutron Research, National Institute of Standards and Technology, Gaithersburg, Maryland 20899-8562, USA*
(Received 11 September 2008; published 29 December 2008)

Inelastic neutron-scattering measurements were carried out on condensed bulk and confined molecular oxygen. The phase transitions of the oxygen confined in cylindrical pores with diameter of ≈94 Å are suppressed below their bulk temperatures or in the case of the lowest-temperature transition to the α phase are suppressed entirely. This last observation is possibly due to the low latent heat of transition for this transition. Both elastic and inelastic neutron-scattering data indicate a mixing of oxygen crystal phases upon confinement. Magnetic ordering fluctuations in the β phase are found to have similar energy-dependent profiles for confined and bulk excitations showing that the magnetic correlation function decay is unaffected by the finite crystal size in confinement.

DOI: 10.1103/PhysRevB.78.214304 PACS number(s): 61.05.fg, 61.43.Gt, 63.22.Kn, 64.60.an

I. INTRODUCTION

Molecular oxygen is a diatomic molecule whose two unpaired electrons give it a magnetic moment and are responsible for its unusual properties when condensed. The bulk liquid phase ($54.4\ \mathrm{K} \leq T \leq 88\ \mathrm{K}$) displays paramagnetic susceptibility, as does the highest temperature solid γ phase ($43.8\ \mathrm{K} \leq T \leq 54.4\ \mathrm{K}$).[1–3] The lowest-temperature solid phase, the α phase (≤ 23.9 K), is an unusual antiferromagnet, as it is a single element insulator whose long-range magnetic order (as observed using polarized neutron scattering[4]) comes from the direct overlap of magnetic orbitals. The β phase $23.9\ \mathrm{K} \leq T \leq 43.8\ \mathrm{K}$ displays antiferromagneticlike behavior in magnetic-susceptibility measurements, but no long-range magnetic ordering is observed from neutron-diffraction measurements.[1,5,6] Energy-resolved polarized neutron-scattering data have shown scattering of magnetic origin that was interpreted as being due to magnetic correlations that decay with time.[4,6,7] As these correlations are at the same wave vector as the eventual long-range magnetic order in the α phase they can be identified as a "precursor" of that phase; indeed, from the low-temperature direction these fluctuations have been shown to stabilize the β phase, reducing the temperature of the α-β transition below that which it would be if the β phase were purely paramagnetic.[8] More recently, static correlations were found from elastic-scattering measurements with superior energy resolution, although the width of the peaks suggests short-range rather than long-range order.[7] The γ phase has a cubic structure with eight molecules per unit cell whose molecular orientation is disordered. The β phase has a rhombohedral structure with no long-range magnetic order; equivalently, a monoclinic cell can be used to describe the structure. The α phase has a monoclinic cell and has long-range magnetic order whose periodicity corresponds to twice the nuclear cell size. The β-α transition is primarily a magnetic transition, the accompanying lattice distortion being quite small. A comprehensive review of the properties of solid oxygen is given in Ref. 9.

Magnetic interaction energy forms a significant fraction of the total binding energy in condensed oxygen, 10% of total as opposed to 1% for conventional magnets.[10] This means that all excitations, phonons, librons and magnons, and the resulting macroscopic properties are inextricably linked to each other. Disentangling these effects to provide a clear root of oxygen's properties has proven challenging.

In this work we are concerned with the effect that confinement within nanometer-scale pores has on the properties of condensed oxygen. Primarily, we aim to show the effects on the generalized vibrational density of states. However, secondary observations regarding phase-transition temperatures and phase structures will be discussed. Confinement is well known to alter the physical properties of liquids and solids. Most obviously, phase-transition temperatures are changed, the sign and magnitude of the change depending on surface energies, latent heats, and pore radii. There is often hysteresis between freezing and melting and new crystalline structures are induced. For a selection of examples, see Refs. 11–17. Oxygen in confinement has received attention previously.[11,13,18–20] Specific-heat measurements of oxygen in a silica xerogel showed the expected transition point depression and hysteresis.[13] Birefringent optical techniques on oxygen in porous Vycor glass indicated faster relaxation in smaller pores and further confirmed that the freezing point depression for confined oxygen is proportional to the inverse of the pore radius.[11] Neutron-diffraction studies were carried out for oxygen in Vycor[21] and xerogel.[18] In Vycor the oxygen structure was found to be similar to the bulk structure, save for an often-observed amorphous component assumed to be at the pore walls. Similar results were found in xerogel; in both studies the crystallite sizes from peak widths were found to be significantly larger then the pore size, suggesting that nucleation may occur in one pore followed by crystallization into adjacent pores. At the lowest temperature and in 35 Å pore diameter, no crystalline peaks were observed. Indeed, the diffraction patterns suggested less order than in the liquid form. There seems to be some disagreement on this last point, however.[20] Wide angle x-ray scattering measurements in porous silica glasses[19] and templated silica glasses with regular cylindrical pores[20] confirmed the change in transition temperatures: both liquid-solid and the γ-β solid-solid transition temperatures were below the bulk values, with the freezing temperatures being consistently below the melting

temperatures. The normal dependence of transition temperature with inverse pore radius was observed. As far as we are aware, the low-temperature α phase has not been directly observed in confinement; in the course of this paper we will consider possible reasons for this.

Recently, work has been published on magnetic-susceptibility measurements on oxygen confined in the porous glass MCM-41.[22] This work focuses mainly on partially filled pores at a range of oxygen partial pressures. The two-dimensional (2D) antiferromagnetic ordering that has been inferred for oxygen adsorbed onto graphite[23,24] is generalized into spin nanotubes.

A number of papers have been published describing the physics of oxygen adsorption onto carbon nanotubes.[25,26] One of these recorded the neutron-diffraction pattern along with the adsorption isotherm for oxygen in bundles of carbon nanotubes.[26] They find that the oxygen preferentially adsorbs onto grooves between the nanotubes. At approximately monolayer coverage they do not observe the neutron-diffraction peak associated with antiferromagnetic ordering. The antiferromagnetic ordering is therefore not ubiquitous feature of quasi-two-dimensional (quasi-2D) oxygen; it presumably can depend on the monolayer geometry and surface chemistry.

This work also forms part of an ongoing effort to explore possibilities for advanced moderating materials to be used in the production of very low-energy neutrons. The prospect of such a source has long been considered of interest since scattering experiments using longer wavelength neutrons allows correlation functions over larger length scales to be determined. Good moderating materials for such a source must have large densities of vibrational states at low energies when equilibriated at low temperatures. Confinement is potentially one way of perturbing the density of states of a material to achieve this goal.

II. EXPERIMENTAL DETAILS

A. Materials

SBA 15 porous silica glass was prepared as described in Ref. 27. The phase purity and crystallinity of the obtained samples were established with powder x-ray diffraction, nitrogen adsorption-desorption measurements, and transmission electron microscopy (TEM) analysis techniques. From nitrogen adsorption experiments a sharply peaked pore size distribution was found with a peak pore diameter of 94 Å using a modified Kelvin equation approach suggested by Kruk *et al.*;[28] the data used to determine this diameter is presented in Sec. III B.

B. Experimental procedure

Neutron-scattering measurements were carried out on the disk chopper spectrometer (DCS) at the National Institute of Standards and Technology (NIST) Center for Neutron Research (NCNR). This is a direct geometry, multichopper, and time-of-flight (TOF) spectrometer, viewing a cold neutron source on the NIST 20 MW reactor.[29] The incident neutron beam on DCS is defined using pulsing and monochromating choppers; we used incident neutrons with energy of 15.5 meV, corresponding to a wavelength of 2.3 Å or wave vector of 2.73 $Å^{-1}$. The sample cells were mounted on an "orange" helium-flow cryostat. The bulk sample was condensed in an annular cell with outer diameter of 12.5 mm and inner diameter of 10.5 mm, giving an annular thickness of 2 mm. The powder sample was loaded into a cylindrical cell with diameter of 12.5 mm. Both cells were 110 mm high and a beam mask was used to restrict the beam incident on the cell to be 90 mm high and 10 mm wide. 2.04 g of dried SBA-15 powder was loaded into the sample cell within a helium glovebox prior to mounting in the cryostat. Oxygen gas was introduced into the cell at 94 K. We loaded the oxygen into the powder in discrete amounts of between 0.005 and 0.001 mol, allowing time between each loading for the system to come to equilibrium. At full loading there was 0.066 mol (2.11 g) of liquid oxygen in the pores. This corresponds to $P/P_0 \approx 0.85$ and as such, the capillary condensation is complete and no bulk oxygen should be present. Data were collected for several runs: (1) a background measurement on the annular sample holder; (2) experimental runs on bulk oxygen in the annular sample holder at three temperatures; (3) a background measurement on the cylindrical sample holder filled with SBA-15 powder; (4) experimental measurements from the cylindrical sample holder filled with SBA-15 powder loaded with oxygen; and (5) a vanadium sample for detector normalization.

C. Data analysis

First, the detector intensities measured at an angle φ and time of flight t, $I(\varphi,t)$, are converted using an interpolation routine into intensities at scattering vector Q and energy E, $I(Q,E)$. Next, those intensities are normalized to the incoming neutron flux Φ, the detector solid angle $\Delta\Omega$ and efficiency η, and the energy-transfer per data channel ΔE. Conventional absolute analysis requires that these also be normalized to the number of atoms in the beam which was not done initially in this case. This then gives the known number of atoms normalized double-differential scattering cross section,

$$\frac{\partial^2\sigma}{\partial\Omega\,\partial E} = \frac{I(Q,E)}{\Phi\Delta\Omega\,\eta\Delta E}. \tag{1}$$

The angle-dependent scattering function can then be calculated according to the conventional scattering law equation,

$$\frac{\partial^2\sigma}{\partial\Omega\,\partial E} = \frac{\sigma_{\mathrm{coh}}}{4\pi}\frac{k_1}{k_0}S(Q,E). \tag{2}$$

The elastic-scattering function $S_{\mathrm{el}}(Q)$ for the material in question can be calculated by integrating $S(Q,E)$ over energy. For the present data this was done between the limits $E=\pm 1$ meV, which is approximately the energy resolution at the elastic peak.

The next step is to calculate a generalized density of vibrational states, $G(Q,E)$, using the identity,[30,31]

$$S_{c,+1}(Q,E) = e^{-2W}\frac{\hbar^2 Q^2}{2\bar{M}E}\langle n+1\rangle G(Q,E), \quad (3)$$

where the subscript "$c,+1$" indicates that this is coherent one-phonon scattering; $2W=(Q^2\langle u^2\rangle)/3$ is the Debye-Waller factor; $\bar{M}$ is the mass of the vibrating unit (for molecular oxygen this is 32 Da); and $\langle n+1\rangle=[1-\exp(-E/k_BT)]^{-1}$ is a thermal population factor. Equation (3) arises after using the *incoherent approximation* when applied to the full expression of one-phonon coherent scattering function. This approximation states that when averaged over a significant Q range, the interference effects (essentially, the "coherence" of the scattering) in the full expression cancel out leaving a scattering function equivalent to the incoherent one-phonon-scattering function. The effective vibrational density of states is then defined by

$$G(E) = \frac{1}{(Q_2-Q_1)}\int_{Q_1}^{Q_2} G(Q,E)dQ. \quad (4)$$

These routines are available as standard software at the NCNR.[32]

III. RESULTS AND DISCUSSION

A. Scattering from bulk O_2

Figure 1 shows full scattering data $S(Q,E)$ collected for the three phases of bulk oxygen as measured on DCS. Similar $S(Q,E)$ maps have been presented before for α and β oxygen,[4–6] but usually in more restricted ranges that highlight specific features. The main inelastic feature in α oxygen is the gapped excitation peak at $\approx$1.3 Å^{-1} and $\approx$10 meV, which was identified with a peak in the magnon density of states. The magnetic nature of this feature was confirmed experimentally using polarized neutron scattering,[4] where it was also shown that the magnon density of states is dominated by in-plane interactions. The long-range in-plane antiferromagnetic ordering is seen in the relatively strong features at $\approx$1.32 and $\approx$1.59 Å^{-1} in the elastic-scattering function (Fig. 2). It is well known that the main difference between α and β oxygen is the introduction of long-range antiferromagnetic ordering in α oxygen, which is marked in these data by the conspicuous absence of those peaks for β oxygen. The similarity of the lowest Q nuclear Bragg peaks for α (1.68, 2.25, and 2.42 Å^{-1}) and β (1.68, 2.25, and 2.46 Å^{-1}) confirms the relatively weak structural transition that occurs between these phases as described in Sec. I. β oxygen has an inelastic feature that is not connected to an elastic peak at 1.3 Å^{-1}. This feature has been noted in connection with magnetic fluctuations and as a precursor to the long-range antimagnetic structure which develops at the same wave vector in α oxygen. A more detailed analysis of the dynamic magnetic correlations signified by this feature will be presented later in the paper.

Elastic magnetic scattering was seen at 0.84 and 1.13 Å^{-1} in the work of Chahid *et al.*[7] but not in our elastic diffraction pattern. This is potentially due to the weak nature of this scattering and the need for finer energy resolution to be able to identify the elastic scattering presented there.

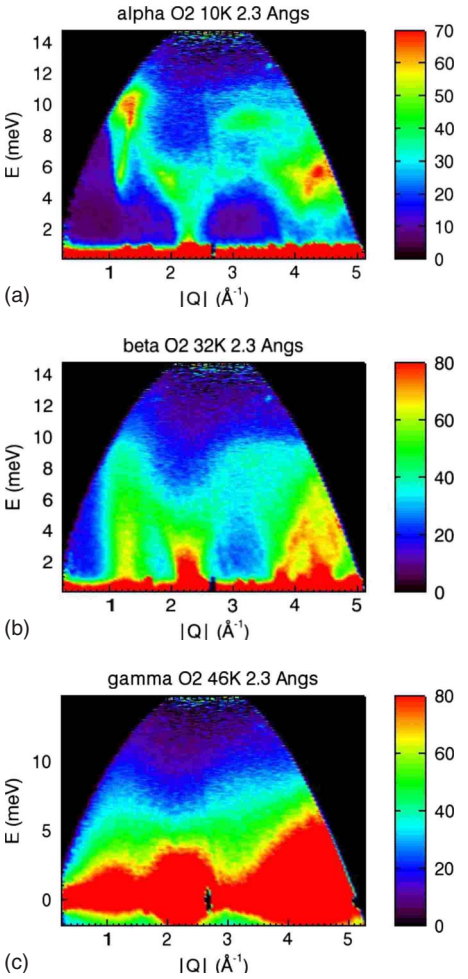

FIG. 1. (Color online) [(a)–(c)] $S(Q,E)$ for bulk oxygen in the three condensed solid phases.

B. Elastic scattering from confined O_2

A nitrogen adsorption isotherm for the SBA-15 used in the neutron experiment is shown in Fig. 3. It is worth pointing out that this is the actual sample used in the scattering measurements, so the absolute values of gas molecules are pertinent. Nitrogen was used instead of oxygen to allow conventional pore radius or surface area analysis. The capillary

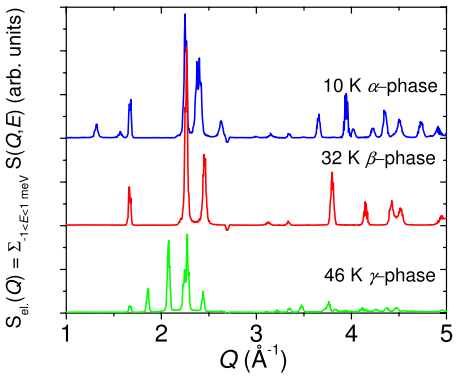

FIG. 2. (Color online) Elastic-scattering function for bulk oxygen in the three condensed solid phases.

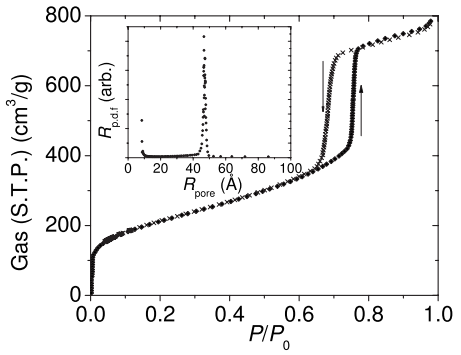

FIG. 3. Nitrogen adsorption and desorption isotherms at 77 K for the SBA-15 porous silica glass used for the neutron-scattering experiment. Inset shows pore radius probability distribution function.

adsorption branch shows a very steep rise, indicative of the narrow distribution of pore radii expected for templated silica glasses. The inset shows this in terms of pore radii from a modified Kelvin equation,[28] the peak being at 47 Å. The total surface area from Brunauer-Emmett-Teller (BET) analysis[33] is 750 m^2/g. The nitrogen isotherm can broadly be separated into two sections: first, the nitrogen that is adsorbed onto the surface (~0–430 cm^3/g); and second, the nitrogen that "capillary condenses" directly (~430–690 cm^3/g). The proportion of nitrogen that is condensed due to the second mechanism is therefore 38%.

The elastic structure factor for confined oxygen is shown in Fig. 4. This plot is achieved by subtracting the scattering function due to the SBA-15 powder from the scattering function due to the powder loaded with oxygen. At the highest temperature shown (46 K), the $S(Q)$ is still liquidlike. At 40 and 35 K there are peaks associated with the γ phase (1.86, 2.07, and 2.28 $Å^{-1}$) superimposed on top of an amorphous background. It should be noted that at 35 K the oxygen is 8.8 K below its bulk γ-β transition. At 30 K there is clear indication of the development of a peak at 1.68 $Å^{-1}$, together with a peak at 3.78 $Å^{-1}$, both of which are characteristic of the β phase. At 30 K there is still evidence of the feature at 2.07 $Å^{-1}$ which is present in the γ but not in the β phase, leading to the conclusion that at this temperature in this measurement there is some coexistence of phases. Below this

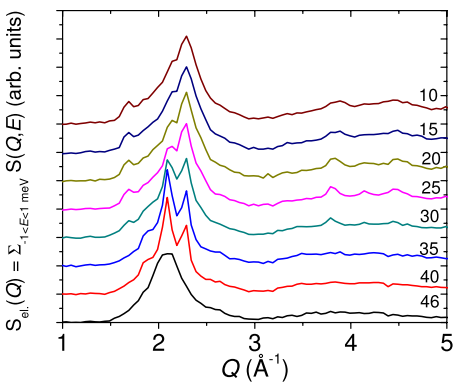

FIG. 4. (Color online) Elastic-scattering function for confined oxygen at a range of temperatures.

temperature we observe a slight sharpening and increasing of the features associated with the β phase and a relative decrease in the intensity of the peak at 2.07 $Å^{-1}$. It should be noted, however, that even at 10 K there is still a little bump above noise on the low-Q side of the wide peak centered at 2.28 $Å^{-1}$ which may be a separate "amorphous" peak that has moved slightly from the peak value at 46 K and sharpened somewhat due to solidification. Alternatively, it may be evidence of a small remnant of γ phase. We also note here the slight discrepancy between this peak reported centered at 2.28 $Å^{-1}$ and the corresponding bulk peak at 2.25 $Å^{-1}$. The statistics collected in the current experiment are not sufficient to unambiguously identify a real difference as the current experiment was not designed to be a crystallographic diffraction study. We must therefore leave open the question of lattice distortion in the β phase due to confinement. From the above description two main points stand out: first, there is clearly a significant amorphous component to the confined oxygen; second, even at 14 K below the bulk β-α transition there is no evidence of the long-range magnetic ordering characteristic of that phase. In relation to the first of these observations, we ask the question as to whether we are able to estimate the amorphous fraction. The answer is not trivial because we cannot perform a simple superposition of weighted bulk scattering functions. The confined crystalline phase is distinct from the bulk crystalline phase because of the finite-sized width of the peaks. There is also a significant interfacial surface between the crystalline fraction taken to be at the center of the pore and the amorphous fraction at the surface. This means that a significant fraction of the terms adding toward the total structure factor will reflect atoms that have correlations with both crystalline and noncrystalline structures. Figure 5(a) shows $S(Q)$ for confined oxygen at 40 K, which is partly crystalline, and also the liquid form at 46 K multiplied by 0.7; also shown are the results assuming that $S(Q)$ at 46 K accurately represents the shape of the amorphous component at 40 K. We are therefore assuming that the shift in structure factor peak due to cooling is negligible. Following the above reasoning, the structure factor of the crystalline component is given by $S_{cryst}(Q,40\ K) = S_{tot}(Q,40\ K) - \kappa S_{tot}(Q,46\ K)$, where κ is the amorphous fraction. This is shown in Fig. 5(b) for $\kappa=1$, 0.9, 0.8, and 0.7. $\kappa=1$ would mean that there is the same amount of amorphous material in the pores at 40 K as at 46 K. This would require that the density increases for both components allowed more oxygen into the path of the neutron beam—enough to replace that which crystallizes. If it is stipulated that the crystalline phase cannot have negative $S(Q)$ at any point then $\kappa=0.7$ is the amorphous fraction. It is interesting to note that this is just slightly larger than the fraction of oxygen adsorbed onto the surface before capillary condensation happens. It occurs to us that this may reflect a different packing that exits for the adsorbed and the capillary condensed oxygen; perhaps the initially adsorbed gas is packed more densely and so is less mobile and therefore less likely to be a real freezable liquid.

The second observation above, the lack of an α phase in confinement, has been noted before.[18,34] It is claimed that magnetic-susceptibility measurements, however, do show the transition to the α phase;[35] some members of the same group

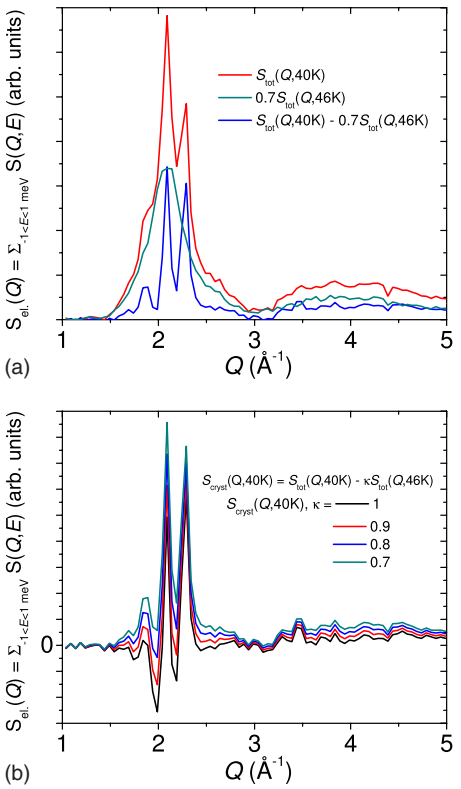

FIG. 5. (Color online) Elastic-scattering function for confined oxygen. (a) Shown are plots of the partially crystalline confined oxygen at 40 K and the liquidlike oxygen at 46 K multiplied by a factor of 0.7; in addition, the difference between these two is shown, being equal to the crystalline component assuming 30% crystallinity. (b) The elastic-scattering function at 40 K due to the crystal component is plotted assuming a range of amorphous fractions κ.

performed x-ray diffraction measurements and suggested that some peak splitting associated with the transition is observable.[19] We do not observe the long-range magnetic ordering associated with the α phase even at 10 K, some 13.9 K below the bulk transition. One possible reason for this is that in confinement the transition temperature change is always a function of the ratio between some surface energy (either between the two transition phases or their respective energies with a third amorphous phase) and the volume energy change, the latent heat.[11,16] The surface energies are difficult to define but the latent heats are well documented. The transition latent heats are 444, 742, and 92 J/mol for the liquid-γ, γ-β, and β-α transitions, respectively; these values were the most recent listed in Ref. 36. The fractional change in transition temperature is inversely proportional to the latent heat per volume.[11,16] Note that the surface energies are different in the two examples referenced because of the different models used, but the statement with regards to the latent heat is still correct. Hence, because the latent heat is small, it is likely that the temperature change for the β-α transition is large. The above argument is necessarily qualitative because we do not know the surface energy between the solid phases in oxygen, but it may explain the lack of α phase in confinement. For example, assuming that the solid-

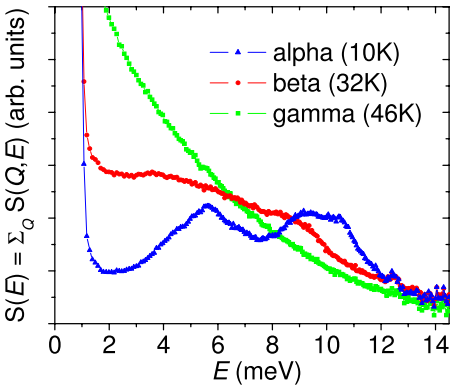

FIG. 6. (Color online) Energy-dependent scattering function for bulk oxygen in the three condensed solid phases. This is calculated by integrating $S(Q,E)$ between 1 and 5 Å^{-1}. Error bars are commensurate with symbol size.

solid surface energies are equal for γ-β and β-α surfaces, we are left with the equation, for a given pore radius, $(\Delta T/T_0) = (kV_m/\Delta h)$, where Δh is the latent heat of the phase transition and V_m is the molar volume of the daughter crystal $\Delta T = T_0 - T$, where T is the temperature of the confined transition, T_0 is the bulk equilibrium melting/freezing temperature, and k is a constant of proportionality. For oxygen $V_m = 21.12$ and 20.6 cm^3/mol for β and α crystals, respectively.[36] For cylindrical pores with diameter of 90 Å (close to our value of 92 Å) $\Delta T/T_0$ is found to be 0.27 for the γ-β transition.[20] Using the values and assumptions listed above this would mean that $\Delta T/T_0 = 2.145$ for the β-α transition and, hence, it would never be seen. The biggest assumption here is the equal surface energies since the γ-β transition has a greater lattice change than the β-α one, indicating that some difference is likely. Nevertheless, as a first approximation and as an illustrative scenario we think the comparison has merit.

C. Inelastic scattering

Inelastic-scattering functions for bulk oxygen in the three solid phases are shown in Fig. 6. These $S(E)$s are defined by integrating $S(Q,E)$ from $Q=0$ to 5 Å^{-1}. The sharp rise at ~1 meV comes from the elastic line. The data for the higher-temperature γ phase are similar to those reported earlier, resembling a broad quasielastic scattering function.[7,37] From Fig. 1(b) it can be seen that the inelastic spectrum from β oxygen has more detailed inelastic structure. In Fig. 6 β oxygen shows a broad hump of greater intensity between 3 and 10 meV and α oxygen has two intense features at ≈5.5 and ≈10 meV—these can be identified from Fig. 1(a) as coming from features at $Q \sim 4.5$ and 1.3 Å^{-1}, respectively.

To directly compare the $S(E)$s from confined oxygen with those from bulk oxygen, they have to be renormalized to account for three factors: (1) the different amounts of O_2 in the two samples; (2) the different proportions of the sample (and therefore total masses given above) illuminated by the neutron beam; and (3) different self-shielding factors from the two samples. For the first correction, we know that the amount of bulk oxygen is 4.53 g and the amount of confined

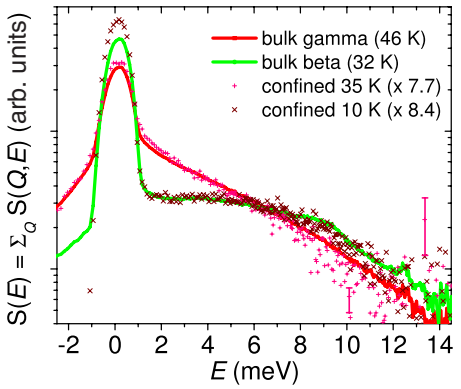

FIG. 7. (Color online) Energy-dependent scattering function for confined oxygen at 35 and 10 K as well as those from bulk β and γ phases. This is calculated by integrating $S(Q,E)$ between 1 and 5 Å^{-1}. Representative error bars (± 1 σ) are shown.

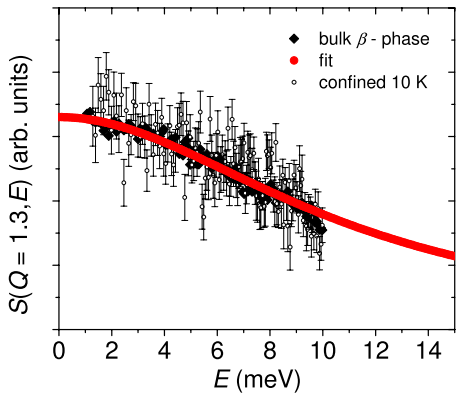

FIG. 8. (Color online) $S(Q=1.3$ Å$^{-1},E)$ for bulk β oxygen and confined oxygen at 10 K. The fit is a Lorentzian centered at 0 meV with HWHM=10.9 meV. Error bars represent one standard deviation based upon counting statistics.

oxygen is 2.11 g, giving a ratio of 0.47. The dimensions of the cells and the beam size are given in Sec. II B; the proportion of the confined sample in the beam is 0.9 that for bulk in the annular cell is 0.59, giving a ratio of 1.53. Self-shielding factors of 0.93 (bulk) and 0.9 (confined) were calculated using the DAVE program available at NIST,[32] giving a ratio of 0.97. We therefore multiply the bulk scattering functions by 0.68 in order to directly compare them with confined.

Figure 7 shows the inelastic-scattering function integrated from $Q=1-5$ Å^{-1} for confined oxygen at 25 and 10 K, along with those of bulk γ and β oxygen for comparison. The intensities of the confined oxygen are multiplied by factors of 7.7 and 8.4 in order that the values for confined at 25 and10 K are commensurate with those from bulk in the γ and β phases, respectively. These scaling factors have been chosen to demonstrate the obvious similarities between those confined and bulk phases. Indeed, the similarities are the same as those observed for the elastic scattering—the crystal structure at 10 K resembled the bulk β phase superimposed on top of an amorphous fraction. The question then presents itself: what is the effect of that amorphous fraction on the inelastic scattering? First, let us consider the ratio of elastic to inelastic scattering for bulk β oxygen. If we take the elastic scattering to be within ± 1 meV and the total scattering between -10.3 and $+14.7$ meV then the ratio is $I_{\mathrm{el}}/I_{\mathrm{tot}}=0.48$. The same ratio for confined oxygen at 10 K is 0.67. We know that there is some oxygen with β-like crystal structure in the confined oxygen at 10 K, so does this also have the same ratio of elastic to inelastic scattering? If 0.33 of the confined 10 K oxygen scattering is inelastic β-like, this would mean that 0.3 of the total scattering should be bulk elastic β-like. The remaining 0.37 is still elastic of as-yet indeterminate origin. From the elastic scattering at 40 K it appeared that 70% of the elastic structure factor came from amorphouslike correlations, whereas following the reasoning above $37/67=55\%$ of the crystalline scattering comes from an indeterminate (possibly amorphous) origin. What can be concluded is that the shape of the inelastic-scattering intensity with energy from confined oxygen at 10 K is similar to that of β oxygen.

We shall now focus on one interesting feature of the β-oxygen inelastic spectrum—the branch stretching out from the elastic line at 1.3 Å^{-1} which, as discussed in Sec. I, seems to form a precursor to the long-range antiferromagnetic ordering in the α phase. $S(E)$ is shown in Fig. 8 for $Q=1.3$ (integrated over 1.2–1.4 Å^{-1}). What is obvious initially is that the shapes of the bulk and confined spectra are similar despite the statistics for the confined oxygen being significantly worse. The fit shown in the graph is to a Lorentzian peak with half-width at half maximum (HWHM) of 10.9 meV. A Lorentzian line shape for inelastic scattering signifies decaying correlations at a particular wave vector; in this instance the decaying correlations are magnetic in origin. Analogous to this analysis is that often encountered in the decay of self correlations of a particle in liquid due to diffusion. In that instance, the HWHM is identified with DQ^2, where Q is the scattering vector (1.3 Å^{-1} in this instance) and D is the diffusion constant. From a HWHM of 10.9 meV and $Q=1.3$ Å^{-1} a value of $D=9.8$ Å^2 ps^{-1} is reached. It can be seen that the shape is relatively unchanged under confinement.

The effective vibrational density of states $G(E)$ is calculated using Eqs. (3) and (4) and is shown for bulk oxygen in all three phases plus confined oxygen at 25 and 10 K in Fig. 9. The spectrum of $G(E)$ from bulk α oxygen is nominally similar to that published previously[5] in that there is a ridge in the region of 5–6 meV and a peak at ≈ 10 meV. These energies do seem to be slightly higher than those depicted previously; for example, the peak seems to be closer to 9 meV. We point to the fact that the magnon excitation which seems to form the main contribution to this peak has a maximum at 10 meV as evidence that our peak is correctly placed. It should be noted that the data in Ref. 5 were collected on an instrument with significantly better energy resolution (~ 90 μeV), but the Q-range sampled is smaller ($\sim 1-3$ Å^{-1}).

The data from the confined oxygen have significantly more statistical noise. However at the lower energies the data are sufficiently good to make the following observations: (1) neither the $G(E)$ at 25 K nor that at 10 K resembles the α-like oxygen; and (2) assuming that at 10 K there is a β-like

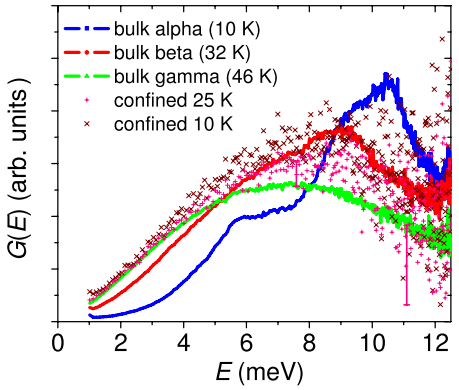

FIG. 9. (Color online) Effective vibrational density of states $G(E)$ for bulk and confined oxygen. Representative error bars ($\pm 1\ \sigma$) are shown.

component (from elastic-scattering measures), the shape of $G(E)$ of this component is not radically altered. Observation 1 is to be expected as we have seen no evidence of α oxygen in confinement. Observation 2 must be qualified by the statement that as above for $S(E)$, the absolute values of $G(E)$ are much lower for the normalized confined oxygen. Figure 10 shows the evolution of $G(E)$ for oxygen in confinement as the temperature is lowered from 46 to 10 K. This is interesting as it shows that the inelastic-scattering response of the oxygen does not change discontinuously, as would be expected from a bulk phase transition. Instead, the magnitude increases gradually in the 6–8 meV region, as is expected going from γ-like to β-like oxygen.

In principle, phonons are collective vibrations of crystal lattices assumed to be infinite; it is therefore intriguing that the shapes of the density of states for confined β-like oxygen (10 K) are similar to that of bulk β oxygen. If the short-range dynamic excitations of magnetic origin at 1.3 Å^{-1} dominated the contributions to $G(E)$ then this similarity would become less puzzling as they would be expected to be affected less by the finiteness of a crystal. From Fig. 1(b) it can be seen that the inelastic scattering contributing to $G(E)$ comes mainly from features at 1.3, 2.3, and above 3.8 Å^{-1}. Furthermore, features in $S(Q,E)$ at high Q contribute pro-

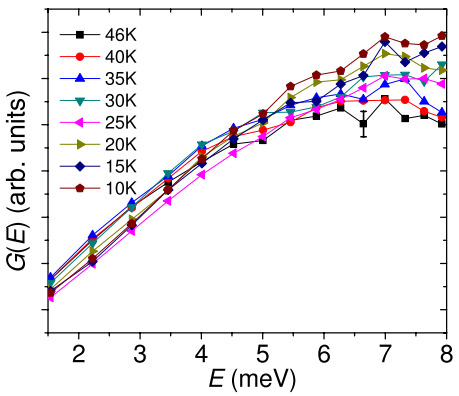

FIG. 10. (Color online) Effective vibrational density of states $G(E)$ for confined oxygen over a range of temperatures. The points plotted are numerical averages of seven adjacent measured data points. Representative error bars ($\pm 1\ \sigma$) are shown.

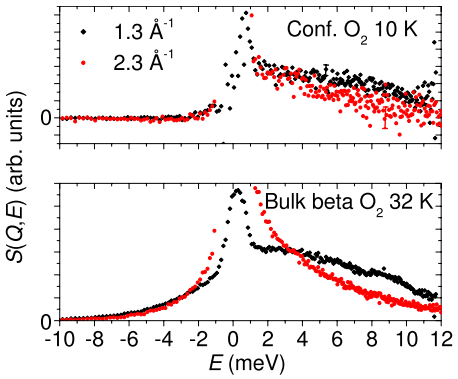

FIG. 11. (Color online) $S(E)$ for $Q=1.3$ and 2.3 Å^{-1} in bulk β oxygen and confined oxygen at 10K. Representative error bars ($\pm 1\ \sigma$) are shown.

gressively less to $G(E)$ due to the $1/Q^2$ weighting term in Eq. (3). Bearing this in mind, Fig. 11 shows $S(E)$ at $Q=1.3$ and 2.3 Å^{-1} for both bulk β oxygen and confined oxygen at 10 K. It can be seen that for bulk oxygen, the feature at 2.3 Å^{-1} has less intensity in absolute terms above approximately 3 meV; it is not unreasonable therefore to assert that $G(E)$ is *dominated* by the feature at 1.3 Å^{-1}. In addition, while the shape of the feature at 1.3 Å^{-1} is relatively unchanged under confinement (see also Fig. 9), the feature at 2.3 Å^{-1} most definitely is. Notably, the intensity at ≈ 1 meV (the edge of the elastic peak) is the same at 2.3 Å^{-1} as it is at 1.3 Å^{-1}, whereas for bulk it is approximately double.

It is notable that in these results we observe no evidence of a boson peak. The boson peak is an excess contribution to the vibrational density of states that is often observed at low meV energies in glassy amorphous materials. It is usually present in plots of $G(E)/E^2$ as a broad peak or hump in the $\approx 2-5$ meV range. Using the elastic-scattering pattern as evidence we have asserted that a significant fraction of the oxygen has an amorphous structure. The lack of a boson peak is therefore intriguing. We have several ideas as to why this should be the case. First, when true glass-forming materials are confined in pores, it is found that the low-energy side of the boson peak is suppressed.[38] This was explained as being due to a maximum allowed phonon wavelength of twice the pore radius. As we are considering the even more restrictive case of a layer around the edge of a pore, it follows that the cut-off energy would be even higher. This may either remove the peak altogether or cause the remaining higher-energy tail to be indistinguishable from the lower-energy crystal phonon density of states. Two other effects may also play a role and are both somewhat entangled in the physics leading to the above reason. First, it is unclear what magnitude the boson peak would have in comparison with the crystal density of states; it may be that for molecular oxygen the intensity is low enough as to make the boson peak negligible. Second, we assume that the glassy layers are strongly influenced by the pore walls so it may be that this perturbs the structure and dynamics to such an extent that the boson peak is suppressed to the point where it is unobservable.

One of the motivating factors in this work was to explore the suitability of nanoconfined materials as moderating ma-

terials for the production of very low-energy neutrons. The main feature one requires for this purpose is a large density of excitations that will remove small amounts of energy from the said neutron beam. Confining oxygen seems to do precisely that. The relative height of $G(E)$ of confined oxygen at 10 K is significantly higher than that for bulk oxygen. It must be remembered that the absolute scattering intensity was much lower for confined oxygen and so any moderating material would have to be thicker, with all the problems for cooling that entails. Nevertheless, as a first step in this direction we have shown that suppressing phase transitions by confinement can lead to enhanced effective vibrational densities of states at low energies.

IV. CONCLUSIONS

In this paper we reported inelastic neutron-scattering measurements on condensed bulk and confined molecular oxygen using the DCS at the Center for High Resolution Neutron Scattering at NIST. The confining medium used was porous silica glass with a narrow pore size distribution and mean pore diameter of 94 Å. The condensed phase-transition temperatures observed in confinement are significantly suppressed below their bulk values. For example, we see evidence of γ-crystal structure 8.8 K below the bulk γ-β transition. As has been observed before, the β-α transition is suppressed entirely in confinement. We speculate that this is because the latent heat energy for this transition, largely magnetic in origin, is relatively low. This means that the overall free-energy driving force is dominated by the surface energy and hence the transition is not seen. We report the generalized vibrational density of states for bulk and confined oxygen and observe that the forms seen here resemble that which would be expected from the structural information from elastic scattering. It is perhaps surprising that this is the case. Phonons and magnons, the excitations which contribute to the generalized vibrational density of states, are usually described as vibrations in infinite lattices. We think that the similarity between the bulk and confined systems is due to them both being dominated by low-Q short-range dynamic excitations of magnetic origin, which are clearly less effected by finite crystal size than long-range excitations.

ACKNOWLEDGMENTS

This work was supported under Department of Commerce Grant No. 70NANB5H1163 and utilized facilities supported in part by the National Science Foundation under Agreement No. DMR-0454672. The porous glasses were prepared by B. Newalkar and S. Komarneni of the Materials Research Laboratory, Pennsylvania State University.

[1] M. F. Collins, Proc. Phys. Soc. London **89**, 415 (1966).
[2] G. C. DeFotis, Phys. Rev. B **23**, 4714 (1981).
[3] F. J. Bermejo, A. de Bernabé, J. L. Martínez, M. L. Senet, G. J. Cuello, S. F. J. Cox, F. Dunstetter, and F. Trow, J. Low Temp. Phys. **111**, 287 (1998).
[4] P. W. Stephens and C. F. Majkrzak, Phys. Rev. B **33**, 1 (1986).
[5] A. de Bernabé, G. J. Cuello, F. J. Bermejo, F. R. Trouw, and A. P. J. Jansen, Phys. Rev. B **58**, 14442 (1998).
[6] P. W. Stephens, R. J. Birgeneau, C. F. Majkrzak, and G. Shirane, Phys. Rev. B **28**, 452 (1983).
[7] A. Chahid, F. J. Bermejo, A. Criado, J. L. Martinez, and M. García-Hernández, J. Phys.: Condens. Matter **5**, 6295 (1993).
[8] B. Kuchta, T. Luty, and R. Meier, J. Phys. C **20**, 585 (1987).
[9] Yu. A. Freiman and H. J. Jodl, Phys. Rep. **401**, 1 (2004).
[10] Yu. A. Freiman and H. J. Jodl, Low Temp. Phys. **28**, 491 (2002).
[11] J. Warnock, D. D. Awschalom, and M. W. Shafer, Phys. Rev. Lett. **57**, 1753 (1986).
[12] C. L. Jackson and G. B. McKenna, J. Non-Cryst. Solids **131-133**, 221 (1991).
[13] E. Molz, A. P. Y. Wong, M. H. W. Chan, and J. R. Beamish, Phys. Rev. B **48**, 5741 (1993).
[14] D. W. Brown, P. E. Sokol, and S. N. Ehrlich, Phys. Rev. Lett. **81**, 1019 (1998).
[15] H. K. Christenson, J. Phys.: Condens. Matter **13**, R95 (2001).
[16] O. Petrov and I. Furó, Phys. Rev. E **73**, 011608 (2006).
[17] C. Alba-Simionesco, B. Coasne, G. Dosseh, G. Dudziak, K. E. Gubbins, R. Radhakrishnan, and M. Sliwinska-Bartkowiak, J. Phys.: Condens. Matter **18**, R15 (2006).
[18] P. E. Sokol, W. J. Ma, K. W. Herwig, W. M. Snow, Y. Wang, J. Koplik, and J. R. Banavar, Appl. Phys. Lett. **61**, 777 (1992).
[19] B. S. Schirato, M. P. Fang, P. E. Sokol, and S. Komarneni, Science **267**, 369 (1995).
[20] D. Wallacher, R. Ackermann, P. Huber, M. Enderle, and K. Knorr, Phys. Rev. B **64**, 184203 (2001).
[21] K. Morishige and Y. Ogisu, J. Chem. Phys. **114**, 7166 (2001).
[22] M. Mito, N. Shinto, Y. Komorida, T. Tajiri, H. Deguchi, S. Takagi, and S. Kohiki, Phys. Rev. B **78**, 064428 (2008).
[23] J. P. McTague and M. Nielsen, Phys. Rev. Lett. **37**, 596 (1976).
[24] M. Nielsen and J. P. McTague, Phys. Rev. B **19**, 3096 (1979).
[25] H. Ulbricht, G. Moos, and T. Hertel, Phys. Rev. B **66**, 075404 (2002).
[26] M. Bienfait, P. Zeppenfeld, N. Dupont-Pavlovsky, M. Muris, M. R. Johnson, T. Wilson, M. DePies, and O. E. Vilches, Phys. Rev. B **70**, 035410 (2004).
[27] B. Newalkar, S. Komarneni, and H. Katsuki, Chem. Commun. (Cambridge) **2000**, 2389.
[28] M. Kruk, M. Jaroniec, and A. Sayari, Langmuir **13**, 6267 (1997).
[29] J. R. D. Copley and J. C. Cook, Chem. Phys. **292**, 477 (2003).
[30] D. L. Price and J. M. Carpenter, J. Non-Cryst. Solids **92**, 153 (1987).
[31] J. M. Carpenter and C. A. Pelizzari, Phys. Rev. B **12**, 2397 (1975).
[32] Downloadable from http://www.ncnr.nist.gov/dave/
[33] S. Brunauer, P. H. Emmett, and E. Teller, J. Am. Chem. Soc. **60**, 309 (1938).
[34] D. D. Awschalom and J. Warnock, Phys. Rev. B **35**, 6779 (1987).

[35] R. Ackermann, T. Knoblauch, D. Kumar, K. Unger, and M. Enderle, J. Low Temp. Phys. **122**, 143 (2001).

[36] V. G. Manzhelii, A. I. Prokhvatilov, V. G. Gavrilko, and A. P. Isakina, *Structure and Thermodynamic Properties of Cryocrystals* (Begell House, New York, 1998).

[37] A. Chahid, M. García-Hernández, F. J. Bermejo, J. L. Martinez, E. Enisco, and F. J. Mompean, Physica B **182**, 409 (1992).

[38] T. Asthalter, M. Bauer, U. van Bürck, I. Sergueev, H. Franz, and A. I. Chumakov, Eur. Phys. J. E **12**, 9 (2003).